Strong- to weak-coupling superconductivity in high-T_c bismuthates: Revisiting the phase diagram via μSR

T. Shang [1,2,*] D. J. Gawryluk [1,†] M. Naamneh,[3,4] Z. Salman [5] Z. Guguchia,[5] M. Medarde,[1]
M. Shi,[3] N. C. Plumb,[3] and T. Shiroka [5,6]

[1]*Laboratory for Multiscale Materials Experiments, Paul Scherrer Institut, Villigen CH-5232, Switzerland*
[2]*Physik-Institut, Universität Zürich, Winterthurerstrasse 190, Zürich CH-8057, Switzerland*
[3]*Swiss Light Source, Paul Scherrer Institut, Villigen CH-5232, Switzerland*
[4]*Department of Physics, Ben-Gurion University of the Negev, Beer-Sheva 84105, Israel*
[5]*Laboratory for Muon-Spin Spectroscopy, Paul Scherrer Institut, Villigen CH-5232, Switzerland*
[6]*Laboratorium für Festkörperphysik, ETH Zürich, Zurich CH-8093, Switzerland*

Several decades after the discovery of superconductivity in bismuthates, the strength of their electron-phonon coupling and its evolution with doping remain puzzling. To clarify these issues, polycrystalline hole-doped $Ba_{1-x}K_xBiO_3$ ($0.1 \leqslant x \leqslant 0.6$) samples were systematically synthesized and their bulk and microscopic superconducting properties were investigated by means of magnetic susceptibility and muon-spin rotation and relaxation (μSR), respectively. The phase diagram of $Ba_{1-x}K_xBiO_3$ was reliably extended up to $x = 0.6$, which is still found to be a bulk superconductor. The lattice parameter a increases linearly with K content, implying a homogeneous chemical doping. The low-temperature superfluid density, measured via transverse-field μSR, indicates an isotropic fully gapped superconducting state with zero-temperature gaps $\Delta_0/k_BT_c = 2.15, 2.10$, and 1.75, and magnetic penetration depths $\lambda_0 = 219, 184$, and 279 nm for $x = 0.3, 0.4$, and 0.6, respectively. A change in the superconducting gap, from a nearly ideal BCS value ($1.76k_BT_c$ in the weak-coupling case) in the overdoped $x = 0.6$ region, to much higher values in the optimally doped case, implies a gradual decrease in electron-phonon coupling with doping.

I. INTRODUCTION

Decades ago, superconductivity (SC) with critical temperatures T_c up to 34 K was discovered in perovskite-type bismuthates [1–3]. Despite extensive studies using various techniques, their pairing mechanism is still under debate [3]. The parent compound $BaBiO_3$ is an insulator, which exhibits charge-density-wave (CDW) order and undergoes multiple structural phase transitions [4–6]. The suppression of the insulating character and of the CDW order upon Ba/K or Bi/Pb substitutions eventually leads to a superconducting phase in $Ba_{1-x}K_xBiO_3$ or $BaBi_{1-y}Pb_yO_3$ [3], with the highest T_c reaching 34 K near $x_K \sim 0.37$ [see Fig. 1(c)]. Neutron powder diffraction measurements show that, for $0.2 \leqslant x \leqslant 0.37$, $Ba_{1-x}K_xBiO_3$ exhibits a cubic-to-orthorhombic phase transition before entering the superconducting phase, while for $x \geqslant 0.37$, the cubic structure persists down to the superconducting phase [7,8]. However, close to $x = 0.32$, a mixture of different phases has also been found [8]. According to our Rietveld refinements of x-ray powder diffraction (XRD) data, samples with $0.1 \leqslant x \leqslant 0.25$ exhibit a mixture of orthorhombic and cubic phases [9]. Later on, it was confirmed that, at

low temperatures, the distortion observed in the superconducting $Ba_{1-x}K_xBiO_3$ samples with $x \sim 0.32$-0.4 is more consistent with a tetragonal symmetry [10]. Systematic studies of the $Ba_{1-x}K_xBiO_3$ crystal structure as a function of doping and temperature are clearly not only in high demand, but also crucial to understand their properties. Indeed, bismuthates rank among the most interesting systems, where the interplay between structural, charge, and electronic instabilities gives rise to new and remarkable phenomena.

According to the phase diagram shown in Fig. 1, the lack of either magnetic order or magnetic fluctuation in bismuthates hints at a nonmagnetic superconducting pairing. To date, two pairing mechanisms, in the two extremes of coupling strengths, have been proposed in order to explain the unexpectedly high T_c of doped bismuthates. One mechanism considers a strong coupling of electrons to high-energy phonon modes, leading to the formation of *polarons*. The polarons then bind into Cooper pairs through a retarded electron-phonon interaction with the low-energy phonon modes [11–13]. Recently, a large electron-phonon coupling constant $\lambda_{ep} > 1$, strong enough to account for the high T_c in $Ba_{1-x}K_xBiO_3$, has been experimentally and theoretically proposed [14,15]. An alternative mechanism suggests that the pairing is mediated by high-energy *charge excitations* [16]. This mechanism does not require a strong coupling; i.e., the superconducting energy gap can be close to $1.76\,k_BT_c$, the canonical weak-coupling BCS-theory value.

014508-1
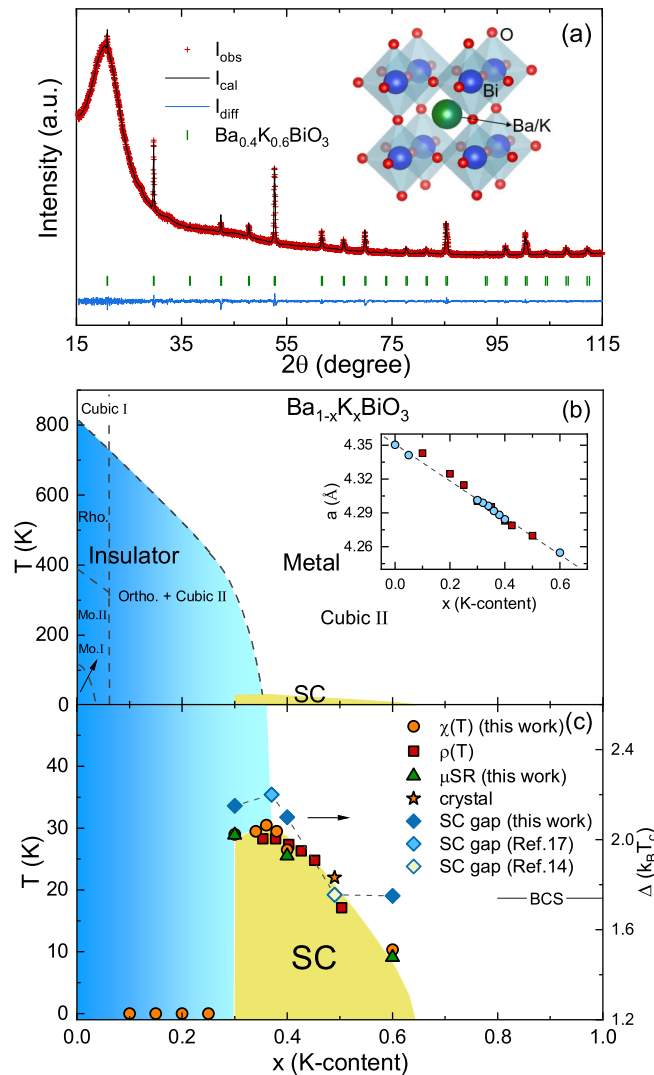
FIG. 1. (a) A typical room-temperature XRD pattern and Rietveld refinements for $Ba_{0.4}K_{0.6}BiO_3$. The crystal structure is shown in the inset. (b) Structural and superconducting phase diagram of $Ba_{1-x}K_xBiO_3$, constructed according to Refs. [3,6,7]. The inset shows the in-plane lattice parameter as a function of K content, with the red symbols referring to data to Ref. [7] and the blue symbols to our XRD data. For $0.1 \leqslant x \leqslant 0.25$, due to a mixture of phases, the relevant lattice parameter is not shown. (c) Enlarged superconducting phase diagram, as obtained from magnetization, μSR, and electrical-resistivity measurements. The evolution with x of the SC gap (generally scaling as the coupling strength) is shown in the right-hand scale. The single-crystal data were taken from Ref. [14], while the electrical resistivity data are from Ref. [7]. The space groups of the different phases are $Fm\bar{3}m$ (cubic I), $R\bar{3}$ (rhombohedral), $P2_1/n$ (monoclinic I), $I2/m$ (monoclinic II), $Ibmm$ (orthorhombic), and Pm-$3m$ (cubic II).

In the case of strong coupling, the energy gap is much larger than the BCS value (for instance, for $x = 0.37$, $\Delta_0 \approx 2.2k_BT_c$ [17]). Upon increasing the K content, the bond/charge disproportionation weakens and eventually it disappears. Nevertheless, the electron pairs may still survive and condense, leading to a superconducting phase, albeit with a reduced T_c value. One could make an educated guess and

suggest a *doping-dependent coupling strength*, a scenario which does not exclude either of the above mechanisms, thus accounting for the widely different experimental results.

To validate the above hypothesis on the evolution of the coupling strength with doping, the study of the superconducting gap and of its symmetry across the entire phase diagram of $Ba_{1-x}K_xBiO_3$ is crucial, in particular in the overdoped region, mostly overlooked due to the lack of high-quality samples. Here, by improving the synthesis conditions, we could obtain high-quality $Ba_{1-x}K_xBiO_3$ samples ($0.1 \leqslant x \leqslant 0.6$), of which those with $x = 0.3$-0.6 show bulk superconductivity. In this paper, we report on the systematic magnetization and muon-spin rotation and relaxation (μSR) investigation of the hole-doped $Ba_{1-x}K_xBiO_3$ system in the range $0.1 \leqslant x \leqslant 0.6$. By using transverse-field (TF) μSR measurements, we study the microscopic superconducting properties, including the gap symmetry, the zero-temperature magnetic penetration depth, and the gap values across the whole superconducting phase region of $Ba_{1-x}K_xBiO_3$ to clearly demonstrate the decrease of the SC coupling strength with doping.

II. EXPERIMENTAL DETAILS

Polycrystalline $Ba_{1-x}K_xBiO_3$ samples were synthesized via solid-state reaction methods [9]. The room-temperature XRD, measured using a Bruker D8 diffractometer, confirmed the samples' purity and the lack of extra phases. The atomic ratios in the various $Ba_{1-x}K_xBiO_3$ samples were measured by x-ray fluorescence (XRF) spectroscopy on an AMETEK Orbis Micro-XRF analyzer. The linear behavior of the in-plane lattice parameter (extracted from the Rietveld refinements; see Fig. 1(a) and the Supplemental Material [9]) vs K content indicates the successful and homogeneous Ba/K substitution in all the studied samples [see inset in Fig. 1(b)]. The magnetic susceptibility measurements were performed on a Quantum Design magnetic property measurement system (MPMS). The bulk μSR measurements were carried out at the general-purpose (GPS), the multipurpose (Dolly), and the high-field and low-temperature (HAL-9500) surface-muon spectrometers at the Swiss muon source of Paul Scherrer Institut, Villigen, Switzerland. The μSR data were analyzed by means of the MUSRFIT software package [18].

III. RESULTS AND DISCUSSION

Characterization of bulk superconductivity. The superconductivity of $Ba_{1-x}K_xBiO_3$ ($0.1 \leqslant x \leqslant 0.6$) was characterized by magnetic susceptibility measurements, performed in a 1-mT field, using both field-cooled (FC) and zero-field-cooled (ZFC) protocols. As shown in Fig. 2(a), the ZFC susceptibility, corrected to account for the demagnetization factor, indicates bulk superconductivity below $T_c = 29.5$, 26.5, and 10.3 K for $x = 0.3$, 0.4, and 0.6, respectively. For $x \leqslant 0.2$, no superconducting transition could be detected down to 1.8 K. For $x = 0.25$, the $\chi(T)$ curve shows a superconducting transition at 25 K with a rather small superconducting fraction (below 1%). The other samples, with a K content between 0.3 and 0.4, exhibit bulk superconductivity, too (see the phase diagram). To perform TF-μSR measurements on superconductors, the applied magnetic field should exceed the lower
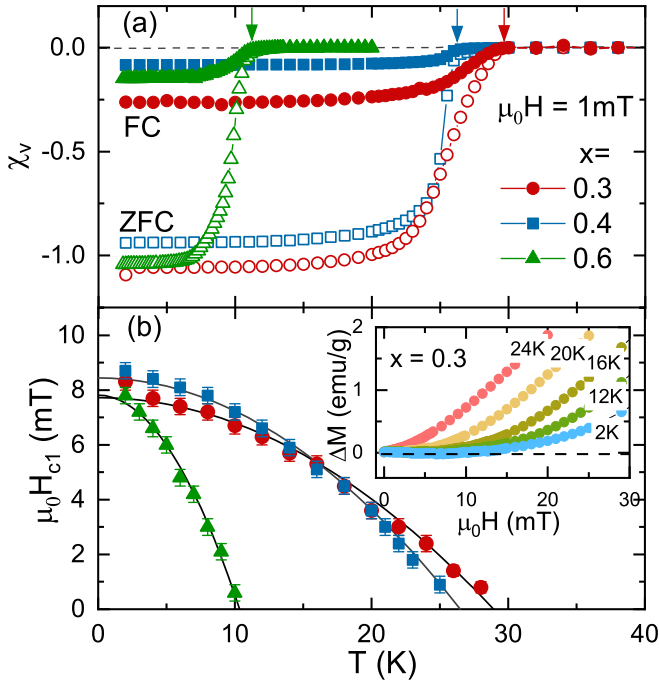
FIG. 2. (a) Temperature-dependent magnetic susceptibility $\chi(T)$ of $Ba_{1-x}K_xBiO_3$ for $x = 0.3$, 0.4, and 0.6. (b) Estimated lower critical field $\mu_0 H_{c1}$ vs temperature. The solid lines are fits to $\mu_0 H_{c1}(T) = \mu_0 H_{c1}(0)[1 - (T/T_c)^2]$. Inset: $\Delta M(H)$ for $x = 0.3$ at selected temperatures; the dashed line indicates the zero value of $\Delta M(H)$. The magnetic susceptibilities were corrected by using the demagnetization factor obtained from the field-dependent magnetization at 2 K (base temperature).

critical field $\mu_0 H_{c1}$, so that the additional field-distribution broadening due to the flux-line lattice (FLL) can be quantified from the muon-spin relaxation rate. To determine $\mu_0 H_{c1}$, the field-dependent magnetization $M(H)$ was measured at various temperatures up to T_c [9]. For each temperature, $\mu_0 H_{c1}$ was determined as the value where $M(H)$ deviates from linearity. The inset of Fig. 2(b) shows $\Delta M(H)$ for the $x = 0.3$ case at several temperatures below T_c. Here, $\Delta M(H) = M(H) - M_{\text{linear}}(H)$, where M_{linear} is the linear low-field magnetization, as obtained from a linear fit to the $M(H)$ data (see Fig. S2 in the Supplemental Material [9]). As indicated by the dashed line, at $\mu_0 H_{c1}$, $\Delta M(H)$ starts deviating from zero value. The $M(H)$ data for all the samples are reported in the Supplemental Material [9]. The estimated $\mu_0 H_{c1}(T)$ values are shown in the main panel of Fig. 2(b) as a function of temperature. The solid lines represent fits to $\mu_0 H_{c1}(T) = \mu_0 H_{c1}(0)[1 - (T/T_c)^2]$ and yield lower critical fields of about 8 mT for all the $Bi_{1-x}K_xBiO_3$ samples (see details in Table I).

Transverse-field μSR. The TF-μSR time spectra were collected at various temperatures up to T_c, following a FC protocol. To track the additional field-distribution broadening due to the FLL in the mixed superconducting state, a magnetic field of 50 mT, i.e., rather large compared to the lower critical fields of $Ba_{1-x}K_xBiO_3$, was applied above T_c. Figure 3(a) shows two representative TF-μSR spectra for $Ba_{0.6}K_{0.4}BiO_3$, collected above and below T_c, with the other samples showing similar features. The enhanced depolarization rate below T_c

TABLE I. Superconducting parameters of $Ba_{1-x}K_xBiO_3$ as determined from magnetization and TF-μSR and fit parameters related to ZF-μSR data collected above and below T_c in $Ba_{0.7}K_{0.3}BiO_3$.

Superconducting parameters vs K doping			
Parameter	$x = 0.3$	$x = 0.4$	$x = 0.6$
$T_c(\chi)$ (K)	29.0	26.5	10.3
$T_c(\mu$SR) (K)	28.9	25.5	9.1
$\mu_0 H_{c1}$ (mT)	7.7	8.4	7.8
Δ_0 ($k_B T_c$)	2.15	2.10	1.75
Δ_0 (meV)	5.35	4.61	1.37
λ_0 (nm)[a]	219	184	279
ZF muon-spin relaxation parameters			
Parameter	at 1.5 K		at 35 K
A_s	0.19982(88)		0.20019(91)
σ (μs^{-1})	0.0105(31)		0.0120(31)
Λ (μs^{-1})	0.0963(35)		0.0881(39)
A_{bg}	0.02724(88)		0.02729(91)

[a]Derived from TF 50 mT μSR measurements.

reflects the inhomogeneous field distribution due to the FLL, causing an additional distribution broadening in the mixed superconducting state, as clearly seen from the fast-Fourier-transform (FFT) spectra shown in Figs. 3(b) and 3(c). Since the relaxations are mostly Gaussian-like, the TF-μSR asymmetry could be modeled by

$$A_{\text{TF}} = A_s \cos(\gamma_\mu B_s t + \phi)e^{-\sigma^2 t^2/2} + A_{bg}\cos(\gamma_\mu B_{bg}t + \phi). \tag{1}$$

Here A_s and A_{bg} represent the initial muon-spin asymmetries for muons implanted in the sample and sample holder (i.e., background), respectively, with the latter not undergoing any depolarization. B_s and B_{bg} are the local fields sensed by implanted muons in the sample and sample holder, $\gamma_\mu = 2\pi \times 135.53$ MHz/T is the muon gyromagnetic ratio, ϕ is the shared initial phase, and σ is a Gaussian relaxation rate. Given the nonmagnetic nature of the sample holder, B_{bg} coincides with the applied magnetic field [see dashed line in Figs. 3(b) and 3(c)] and was used as an intrinsic reference.

In the superconducting state, the measured Gaussian relaxation rate σ includes contributions from both the FLL (σ_{sc}) and a temperature-invariant relaxation due to nuclear magnetic moments (σ_n) (see also ZF-μSR below). The FLL-related relaxation can be extracted by subtracting the nuclear contribution according to $\sigma_{sc} = \sqrt{\sigma^2 - \sigma_n^2}$. For small applied magnetic fields [with respect to the upper critical field H_{c2} ($H_{\text{appl}}/H_{c2} \ll 1$)], the magnetic penetration depth λ can be obtained from $\sigma_{sc}(T)$ [19,20]:

$$\frac{\sigma_{sc}^2(T)}{\gamma_\mu^2} = 0.00371\frac{\Phi_0^2}{\lambda^4(T)}, \tag{2}$$

with Φ_0 the quantum of magnetic flux. For $Ba_{1-x}K_xBiO_3$, H_{c2} is much higher than the applied magnetic field [21,22], implying the validity of the above equation. The derived inverse square of the magnetic penetration depth (proportional to the superfluid density ρ_{sc}) is shown normalized to the zero-temperature values in Fig. 4. The temperature-independent
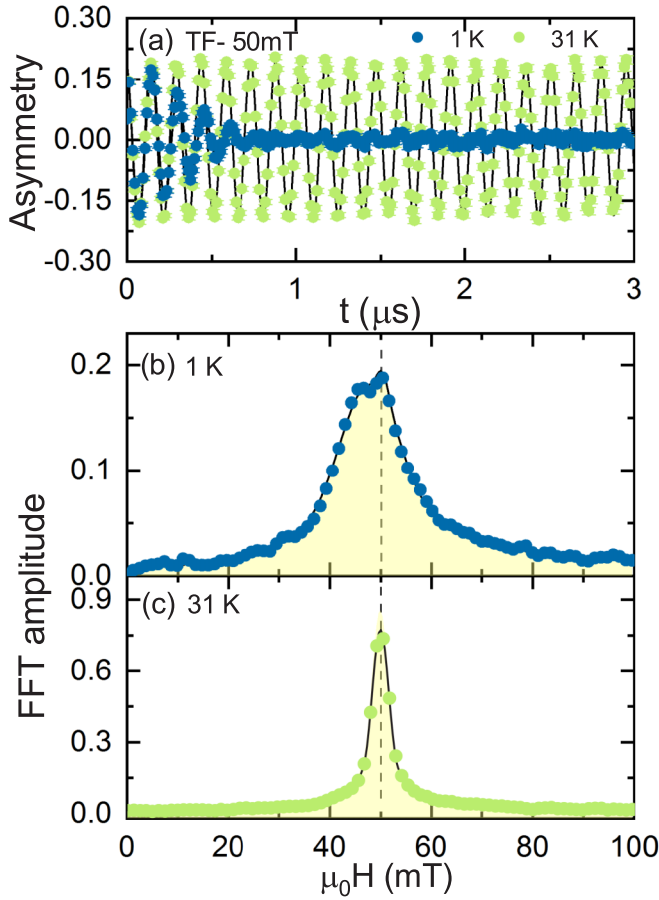
FIG. 3. (a) TF-μSR time-domain spectra for Ba$_{0.6}$K$_{0.4}$BiO$_3$, collected below (1 K) and above (31 K) T_c in an applied field of 50 mT. The other samples exhibit similar features. The fast muon-spin relaxation rate reflects the extra broadening of the field distribution due to the development of the FLL. Fast Fourier transform (FFT) of the above time spectra at (b) 1 K and (c) 31 K. The solid lines in (a)–(c) are fits to Eq. (1) using a single Gaussian relaxation; the dashed line indicates the applied external magnetic field (50 mT). Note the clear diamagnetic shift below T_c in (b).

FIG. 4. Normalized superfluid density vs temperature, as determined from TF-μSR measurements for (a) $x = 0.3$, (b) $x = 0.4$ (b), and (c) $x = 0.6$. The solid lines represent fits to a fully gapped s-wave model (see text). For $x = 0.4$, the GPS data are highly consistent with those reported in Ref. [17] collected in a field of 200 mT. The tiny mismatch between the theoretical value and experimental data near T_c might be related to the broad superconducting transition (see Fig. 2). The fitting parameters are summarized in Table I.

behavior of the superfluid density for $T/T_c < 1/3$ clearly suggests the absence of excitations and, therefore, a nodeless s-wave superconductivity in Ba$_{1-x}$K$_x$BiO$_3$. By converse, for a nodal superconductor, the superfluid density is expected to depend on temperature below $T_c/3$, as examples in p- or d-wave superconductors [23,24]. To gain further insight into the superconducting pairing symmetry of Ba$_{1-x}$K$_x$BiO$_3$, the temperature-dependent superfluid density $\rho_{sc}(T)$ was further analyzed by using a fully gapped s-wave model:

$$\rho_{sc}(T) = 1 + 2 \int_{\Delta(T)}^{\infty} \frac{E}{\sqrt{E^2 - \Delta^2(T)}} \frac{\partial f}{\partial E} \, dE, \qquad (3)$$

where $f = (1 + e^{E/k_B T})^{-1}$ is the Fermi function and $\Delta(T)$ is the superconducting gap function. The temperature variation of the superconducting gap is assumed to follow $\Delta(T) = \Delta_0 \tanh\{1.82[1.018(T_c/T - 1)]^{0.51}\}$ [25], where Δ_0, the zero-temperature gap value, is the only adjustable parameter. The solid lines in Fig. 4 are fits to a single-gap s-wave model, which yields magnetic penetration depths
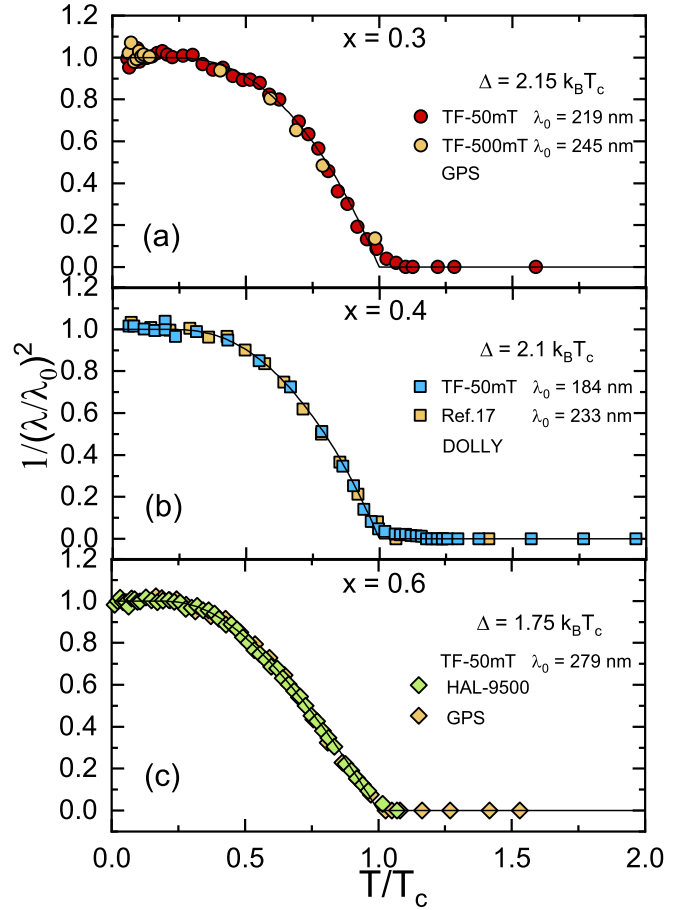
$\lambda_0 = 219(3)$, 184(2), and 279(2) nm, and gap values $\Delta_0/k_B T_c = 2.15(2)$, 2.10(3), and 1.75(3), for $x = 0.3$, 0.4, and 0.6, respectively. The data sets at higher fields (500 and 200 mT for $x = 0.3$ and 0.4, respectively) exhibit almost identical features as those at 50 mT, further confirming the single-gap nature of superconductivity in the Ba$_{1-x}$K$_x$BiO$_3$ family. Close to optimal K doping (e.g., $x = 0.3$ and 0.4), the derived gap values are significantly larger than the BCS value of $1.76 k_B T_c$, while upon overdoping (e.g., $x = 0.6$), the gap is more consistent with the BCS value in the weak-coupling limit. Since normally the SC gap scales with the coupling strength, a progressive increase of K doping in Ba$_{1-x}$K$_x$BiO$_3$, from the optimal- to the over-doped regime, seems to correspond to a change from strong to weak electron-phonon coupling. While from these results one can infer that the overall coupling constant λ_{ep} decreases, this can potentially be weakened also by a reduction in the density of states at E_F, rather than a decrease in the electron-phonon scattering matrix elements *per se* [26]. In any case, the fully gapped state and the strong electron-phonon coupling are also supported by recent photoemission measurements [14].
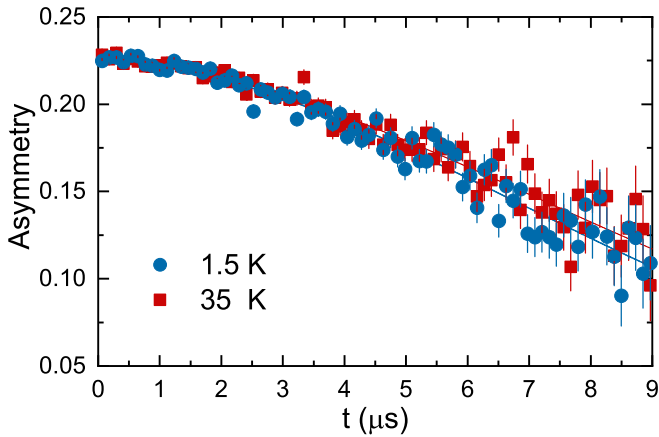
FIG. 5. ZF-μSR spectra in the superconducting (1.5 K) and the normal state (35 K) of $Ba_{0.7}K_{0.3}BiO_3$. Both data sets show only a weak muon-spin depolarization with no visible differences, implying a preserved time-reversal symmetry. The solid lines are fits to the spectra, as described in the text.

The superfluid density and the magnetic penetration depth are intimately linked through the London equation, $\lambda^{-2} = \mu_0 e^2 n_s m^*$, where m^* is the effective mass of quasiparticles and n_s the carrier density (known also as superfluid density in the superconducting state) [27]. The nonmonotonic dependence of the magnetic penetration depth in $Ba_{1-x}K_xBiO_3$ with increasing K doping can be due to either a change of m^* or n_s. With no prior knowledge of how these quantities change with doping, it is not straightforward to explain the observed nonmonotonic dependence of $\lambda(x)$. Nevertheless, from an analogy with other unconventional superconductors, we can still make an educated guess. In the underdoped regime, the cuprates show a linear relationship between the superfluid density and the critical temperature [28,29]. When moving across the optimal doping towards the overdoped regime, this behavior becomes more complex and shows a "boomerang"-like shape (whose origin is still under debate). In $Ba_{1-x}K_xBiO_3$, T_c changes only slightly between $x = 0.3$ and 0.4, while the superfluid density increases substantially (by almost 40%). On the other hand, for $x = 0.6$, both T_c and the superfluid density decrease significantly. To conclude whether a "boomerang"-like (i.e., nonmonotonic) behavior is confirmed also here, further doping values are required. In addition, for an independent access to m^* and n_s, low-T specific heat or Hall resistivity measurements could be very helpful.

Zero-field μSR. To search for possible magnetic features or time-reversal-symmetry (TRS) breaking in the superconducting state of $Ba_{1-x}K_xBiO_3$ we performed also zero-field (ZF) μSR measurements. Representative ZF-μSR spectra collected above and below T_c for $Ba_{0.7}K_{0.3}BiO_3$ are shown in Fig. 5. Here, the absence of coherent oscillations or fast damping is evidence of the nonmagnetic nature of $Ba_{1-x}K_xBiO_3$. Therefore, the weak muon-spin relaxation is mainly determined by the randomly oriented nuclear moments, which can be described by a Gaussian Kubo-Toyabe relaxation function $G_{KT} = [\frac{1}{3} + \frac{2}{3}(1 - \sigma^2 t^2) e^{-\frac{\sigma^2 t^2}{2}}]$ [30,31]. In polycrystalline samples, the 1/3-nonrelaxing and 2/3-relaxing components of the asymmetry correspond to the powder average of the

local internal fields with respect to the initial muon-spin direction. The solid lines in Fig. 5 represent fits to each data set by considering an additional Lorentzian relaxation Λ, i.e., $A_{ZF} = A_s G_{KT} e^{-\Lambda t} + A_{bg}$. Here A_s and A_{bg} are the same as in the TF-μSR case [see Eq. (1)]. The resulting fit parameters are also summarized in Table I. The weak Gaussian and Lorentzian relaxation rates reflect the small nuclear moments in $Ba_{1-x}K_xBiO_3$. In both the normal and the superconducting states, the relaxations are very similar (within the experimental error), as demonstrated by the practically overlapping ZF-μSR spectra above and below T_c. This lack of evidence for an additional μSR relaxation below T_c excludes a possible TRS breaking in the superconducting state of $Ba_{1-x}K_xBiO_3$.

IV. DISCUSSION

In this study we pursued a twofold goal: to reliably extend and revisit the superconducting phase diagram of $Ba_{1-x}K_xBiO_3$ and to reconcile the seemingly contradictory mechanisms put forward to explain its superconductivity.

As for the first point, $Ba_{1-x}K_xBiO_3$ represents a very interesting system among oxide superconductors, to be compared against the cuprates. Prominent differences include the isotropic character of $Ba_{1-x}K_xBiO_3$ and its lack of half-filled d orbitals, in contrast to the two-dimensional nature of cuprates that contain Cu in a $3d^9$ state. However, detailed studies, as the one presented here, have been hampered by the lack of high-quality $Ba_{1-x}K_xBiO_3$ single crystals. Due to the high reactivity and volatility of K_2O, bulk $Ba_{1-x}K_xBiO_3$ samples can only be prepared in a vacuum or dry environment (often at low temperatures), or by means of high-pressure and high-temperature techniques. Our successful systematic synthesis of $Ba_{1-x}K_xBiO_3$ samples with different K-doping values made it possible to reliably construct the $Ba_{1-x}K_xBiO_3$ phase diagram using different techniques and to confirm once more (this time over the whole phase diagram, and not only for one composition, as in Ref. [14]), the *conventional nature* of its superconductivity.

As for the second point, over the years, different experimental techniques (e.g., photoemission, tunneling, and optics) have provided conflicting estimates for the electron-phonon coupling strength λ_{ep} in $Ba_{1-x}K_xBiO_3$. Such enduring controversy has been complicated by the fact that only rarely were high-quality materials available across the whole K-doping range and not always could they be studied systematically. By showing that the coupling regime is doping dependent, our systematic μSR investigation of the entire family finally clarifies this long-standing issue and offers new insights concerning the pairing mechanism in $Ba_{1-x}K_xBiO_3$.

V. SUMMARY

By successfully synthesizing high-quality samples of the $Ba_{1-x}K_xBiO_3$ bismuthates (with x up to 0.6), we could systematically revisit their superconducting phase diagram. Bulk superconductivity in the range $0.3 \leqslant x \leqslant 0.6$ (with $T_c \sim 10$-30 K) was characterized by magnetization measurements, followed by microscopic μSR experiments. The temperature variation of the superfluid density, as determined via TF-μSR, reveals a fully gapped superconductivity in

$Ba_{1-x}K_xBiO_3$, independent of doping and is well described by an isotropic *s*-wave model. At the same time, the derived superconducting-gap values strongly suggest a doping-induced *crossover from strong- to weak-coupling*, a finding which can account for the seemingly contradictory models previously used to explain the superconductivity of the bismuthates. Finally, the lack of spontaneous magnetic fields below T_c, as revealed by ZF-μSR measurements, indicates that time-reversal symmetry is preserved in the superconducting state of $Ba_{1-x}K_xBiO_3$.

[1] R. J. Cava, B. Batlogg, J. J. Krajewski, R. Farrow, L. W. Rupp, A. E. White, K. Short, W. F. Peck, and T. Kometani, Superconductivity near 30 K without copper: The $Ba_{0.6}K_{0.4}BiO_3$ perovskite, Nature (London) **332**, 814 (1988).

[2] L. F. Mattheiss, E. M. Gyorgy, and D. W. Johnson, Superconductivity above 20 K in the Ba-K-Bi-O system, Phys. Rev. B **37**, 3745 (1988).

[3] A. W. Sleight, Bismuthates: $BaBiO_3$ and related superconducting phases, Physica C (Amsterdam) **514**, 152 (2015), and references therein .

[4] F. Munakata, A. Nozaki, T. Kawano, and H. Yamauchi, Electrical conduction in $BaBiO_{3-x}$ at high temperatures, Solid State Commun. **83**, 355 (1992).

[5] H. Sato, S. Tajima, H. Takagi, and S. Uchida, Optical study of the metal-insulator transition on $Ba_{1-x}K_xBiO_3$ thin films, Nature (London) **338**, 241 (1989).

[6] N. C. Plumb, D. J. Gawryluk, Y. Wang, Z. Ristić, J. Park, B. Q. Lv, Z. Wang, C. E. Matt, N. Xu, T. Shang, K. Conder, J. Mesot, S. Johnston, M. Shi, and M. Radović, Momentum-Resolved Electronic Structure of the High-T_c Superconductor Parent Compound $BaBiO_3$, Phys. Rev. Lett. **117**, 037002 (2016).

[7] S. Pei, J. D. Jorgensen, B. Dabrowski, D. G. Hinks, D. R. Richards, A. W. Mitchell, J. M. Newsam, S. K. Sinha, D. Vaknin, and A. J. Jacobson, Structural phase diagram of the $Ba_{1-x}K_xBiO_3$ system, Phys. Rev. B **41**, 4126 (1990).

[8] D. G. Hinks, B. Dabrowski, J. D. Jorgensen, A. W. Mitchell, D. R. Richards, S. Pei, and D. Shi, Synthesis, structure and superconductivity in the $Ba_{1-x}K_xBiO_{3-y}$ system, Nature (London) **333**, 836 (1988).

[9] See Supplemental Material at http://link.aps.org/supplemental/10.1103/PhysRevB.101.014508 for details on the measurements of crystal structure, magnetization, and chemical concentrations, which includes Refs. [6–8].

[10] M. Braden, W. Reichardt, E. Elkaim, J. P. Lauriat, S. Shiryaev, and S. N. Barilo, Structural distortion in superconducting $Ba_{1-x}K_xBiO_3$, Phys. Rev. B **62**, 6708 (2000).

[11] T. M. Rice and L. Sneddon, Real-Space and *k*-Space Electron Pairing in $BaPb_{1-x}Bi_xO_3$, Phys. Rev. Lett. **47**, 689 (1981).

[12] A. S. Alexandrov and V. V. Kabanov, Theory of superconducting T_c of doped fullerenes, Phys. Rev. B **54**, 3655 (1996).

[13] G.-M. Zhao, V. Kirtikar, and D. E. Morris, Isotope effects and possible pairing mechanism in optimally doped cuprate superconductors, Phys. Rev. B **63**, 220506(R) (2001).

[14] C. H. P. Wen, H. C. Xu, Q. Yao, R. Peng, X. H. Niu, Q. Y. Chen, Z. T. Liu, D. W. Shen, Q. Song, X. Lou, Y. F. Fang, X. S. Liu, Y. H. Song, Y. J. Jiao, T. F. Duan, H. H. Wen, P. Dudin, G. Kotliar, Z. P. Yin, and D. L. Feng, Unveiling the Superconducting Mechanism of $Ba_{0.51}K_{0.49}BiO_3$, Phys. Rev. Lett. **121**, 117002 (2018).

[15] Z. Li, G. Antonius, M. Wu, F. H. da Jornada, and S. G. Louie, Electron-Phonon Coupling from *Ab Initio* Linear-Response Theory within the *GW* Method: Correlation-Enhanced Interactions and Superconductivity in $Ba_{1-x}K_xBiO_3$, Phys. Rev. Lett. **122**, 186402 (2019).

[16] B. Batlogg, R. J. Cava, L. W. Rupp, A. M. Mujsce, J. J. Krajewski, J. P. Remeika, W. F. Peck, A. S. Cooper, and G. P. Espinosa, Density of States and Isotope Effect in BiO Superconductors: Evidence for Nonphonon Mechanism, Phys. Rev. Lett. **61**, 1670 (1988).

[17] G.-M. Zhao, Muon spin relaxation and magnetic measurements on $Ba_{0.63}K_{0.37}BiO_3$: Evidence for polaronic strong-coupling phonon-mediated pairing, Phys. Rev. B **76**, 020501(R) (2007).

[18] A. A. Suter and B. M. Wojek, Musrfit: A free platform-independent framework for μSR data analysis, Phys. Procedia **30**, 69 (2012).

[19] W. Barford and J. M. F. Gunn, The theory of the measurement of the London penetration depth in uniaxial type II superconductors by muon spin rotation, Physica C (Amsterdam) **156**, 515 (1988).

[20] E. H. Brandt, Properties of the ideal Ginzburg-Landau vortex lattice, Phys. Rev. B **68**, 054506 (2003).

[21] U. Welp, W. Kwok, G. Crabtree, H. Claus, K. Vandervoort, B. Dabrowski, A. Mitchell, D. Richards, D. Marx, and D. Hinks, The upper critical field of $Ba_{1-x}K_xBiO_3$, Physica C (Amsterdam) **156**, 27 (1988).

[22] S. N. Barilo, S. V. Shiryaev, V. I. Gatalskaya, J. W. Lynn, M. Baran, H. Szymczak, R. Szymczak, and D. Dew-Hughes, Scaling of magnetization and some basic parameters of $Ba_{1-x}K_xBiO_{3+y}$ superconductors near T_c, Phys. Rev. B **58**, 12355 (1998).

[23] I. Bonalde, B. D. Yanoff, M. B. Salamon, D. J. Van Harlingen, E. M. E. Chia, Z. Q. Mao, and Y. Maeno, Temperature Dependence of the Penetration Depth in Sr_2RuO_4: Evidence for Nodes in the Gap Function, Phys. Rev. Lett. **85**, 4775 (2000).

[24] R. Khasanov, A. Shengelaya, A. Maisuradze, F. La Mattina, A. Bussmann-Holder, H. Keller, and K. A. Müller, Experimental Evidence for Two Gaps in the High-Temperature $La_{1.83}Sr_{0.17}CuO_4$ Superconductor, Phys. Rev. Lett. **98**, 057007 (2007).

[25] A. Carrington and F. Manzano, Magnetic penetration depth of MgB_2, Physica C (Amsterdam) **385**, 205 (2003).

[26] P. M. Dee, K. Nakatsukasa, Y. Wang, and S. Johnston, Temperature-filling phase diagram of the two-dimensional Holstein model in the thermodynamic limit by self-consistent Migdal approximation, Phys. Rev. B **99**, 024514 (2019).

[27] M. Tinkham, *Introduction to Superconductivity* (Dover, Mineola, NY, 1996).

[28] Y. J. Uemura, G. M. Luke, B. J. Sternlieb, J. H. Brewer, J. F. Carolan, W. N. Hardy, R. Kadono, J. R. Kempton, R. F. Kiefl, S. R. Kreitzman, P. Mulhern, T. M. Riseman, D. L. Williams, B. X. Yang, S. Uchida, H. Takagi, J. Gopalakrishnan, A. W. Sleight, M. A. Subramanian, C. L. Chien, M. Z. Cieplak, G. Xiao, V. Y. Lee, B. W. Statt, C. E. Stronach, W. J. Kossler, and X. H. Yu, Universal Correlations Between T_c and $\frac{n_s}{m^*}$ (Carrier Density over Effective Mass) in High-T_c Cuprate Superconductors, Phys. Rev. Lett. **62**, 2317 (1989).

[29] C. Niedermayer, C. Bernhard, U. Binninger, H. Glückler, J. L. Tallon, E. J. Ansaldo, and J. I. Budnick, Muon Spin Rotation Study of the Correlation Between T_c and n_s/m^* in Overdoped $Tl_2Ba_2CuO_{6+\delta}$, Phys. Rev. Lett. **71**, 1764 (1993).

[30] R. Kubo and T. Toyabe, *Magnetic Resonance and Relaxation*, edited by R. Blinc (North-Holland, Amsterdam, 1967).

[31] A. Yaouanc and P. D. de Réotier, *Muon Spin Rotation, Relaxation, and Resonance: Applications to Condensed Matter* (Oxford University Press, Oxford, UK, 2011).